Journal of Alloys and Compounds 546 (2013) 129–137

Contents lists available at SciVerse ScienceDirect

Journal of Alloys and Compounds

journal homepage: www.elsevier.com/locate/jalcom

Beneficial effect of carbon on hydrogen desorption kinetics from Mg–Ni–In alloy

J. Cermak [a,*], L. Kral [b]

[a] Institute of Physics of Materials, v.v.i., AS CR, CEITEC IPM, Zizkova 22, CZ-61662 Brno, Czech Republic
[b] Institute of Physics of Materials, v.v.i., AS CR, Zizkova 22, CZ-61662 Brno, Czech Republic

A R T I C L E I N F O

Article history:
Received 11 June 2012
Received in revised form 6 August 2012
Accepted 8 August 2012
Available online 17 August 2012

Keywords:
Energy storage materials
Hydrogen absorbing materials
Metal hydrides

A B S T R A C T

In the present paper, hydrogen desorption kinetics from hydrided Mg–Ni–In–C alloys was investigated. A chemical composition that substantially accelerates hydrogen desorption was found. It was observed that carbon improves the hydrogen desorption kinetics significantly. Its beneficial effect was found to be optimum close to the carbon concentration of about $c_C \cong 5$ wt.%. With this composition, stored hydrogen can be desorbed readily at temperatures down to about 485 K, immediately after hydrogen charging. This can substantially shorten the hydrogen charging/discharging cycle of storage tanks using Mg–Ni-based alloys as hydrogen storage medium. For higher carbon concentrations, unwanted phases precipitated, likely resulting in deceleration of hydrogen desorption and lower hydrogen storage capacity.

1. Introduction

There are numerous reviews summarizing the broad class of hydrogen storage materials (HSMs), e.g., [1–3]. The most recent survey of solid materials for future energy storage can be found in [4,5]. Among the prospective HSMs, Mg-based alloys seem to be of an on-going interest [6,7]. Ball milling [6,8,9] and catalysis [10–20] are effective techniques used to improve the hydrogen storage characteristics of pure Mg. The mechanism of catalytic action and the effective loci of catalyst atoms were studied in papers [21,22]. Transition metals [19,23–27] and their oxides [28–32] were used as catalysts. The most efficient addition element was Ni. A special class of Mg–Ni-based HSMs are alloys containing Mg_2Ni, whose hydrogen storage characteristics were studied, e.g., in papers [33–35]. Other techniques were also applied to improve hydrogen storage properties – for example melt spinning [36,37] and high pressure technique [38].

The present work continues our previous measurements of hydrogen diffusivity in binary Mg–Ni alloys [39], study of catalytic effects [40] and chemical composition of ternary Mg–Ni–X alloys, where X are elements from the 13th and 14th groups [41].

The beneficial influence of carbon on hydrogen sorption in Mg-based materials has been reported in the literature [42–57]. Hydrogen storage in pure Mg was studied in [42–48], hydrogen storage in Mg-based complex hydrides was investigated in [49,50]. Authors of [55] observed improvement of hydrogen absorption of Mg with C only, whereas almost no effect on hydrogen desorption was reported. Several possible mechanisms were proposed in the literature explaining the observed influence of carbon on the sorption characteristics of Mg and Mg–Ni alloys. Carbon is considered an anti-sticking agent [54] that prevents agglomeration, bonding and welding of Mg particles in ball-milling. Carbon is thus believed to facilitate fine ball-milling and production of powder of smaller grains. Authors of papers [55,56] conclude that carbon provides Mg alloys with enhanced resistance to oxidation. It was also found that carbon enhances the density of matrix defects, which may decrease the hydride decomposition temperature. Catalytic [51,53] and synergic effects of carbon and other alloy components [52,54] result in improved hydrogen desorption from various HSMs. A large number of dangling bonds of carbon generated during milling was reported [51] as sites of easy hydrogen absorption. In [57], a limiting carbon concentration was reported: The authors concluded that addition of more than 9 wt.% of graphite to Mg–V fine powder did not lead to any further acceleration of hydrogen absorption.

The aim of the present paper is to find improved hydrogen desorption characteristics of chosen Mg–Ni-based ball-milled alloys containing In, which effectively enhances resistance to oxidation [41]. The influence of graphitic carbon on the hydrogen desorption kinetics was tested.

2. Experimental

2.1. Experimental alloys – Preparation and thermal treatment

Samples were prepared in *Fritsch Pulverisette6* ball-mill using fine splinters of pure Mg (typical thickness was about 100 μm, purity 99.98%), Ni powder (grain size 3–7 μm, purity 99.9%) and In powder (grain size 150 μm, purity 99.99% except for 1% of Mg added to In as an anticaking agent). Carbon powder to be used as an additive was prepared by crushing spectroscopic-pure carbon lumps in a mortar. The mass ratio of the milling balls to the blend milled was about 60 and the milling cycle – 10 min milling/50 min cooling – was repeated 20 times.

* Corresponding author. Tel.: +420 532 290 422; fax: +420 541 218 657.
E-mail address: cermak@ipm.cz (J. Cermak).

0925-8388/$ - see front matter © 2012 Elsevier B.V. All rights reserved.
http://dx.doi.org/10.1016/j.jallcom.2012.08.037

Table 1
Average chemical composition of experimental alloys.

Material	Concentration in wt.%				c_C/c_{Mg}	$c_{Ni}/(c_{Ni} + c_{Mg})$	Note
	c_{Mg}	c_{Ni}	c_{In}	c_C			
E	76.49	23.51	–	–	–	0.24	Eutectic
E–In	72.40	16.86	10.74	–	–	0.19	Alloyed eutectic
E–0.14C	72.65	16.92	–	10.43	0.14	0.19	
E–In–0.07C	68.91	15.94	10.21	4.94	0.07	0.19	
E–In–0.14C	65.68	15.20	9.74	9.38	0.14	0.19	
Ea–In–0.14C	67.86	12.92	9.80	9.41	0.14	0.16	
Eb–In–0.14C	69.63	10.37	10.05	9.95	0.14	0.13	
E–In–0.22C	62.64	14.58	9.28	13.50	0.22	0.19	
E–In–0.29C	60.00	13.90	8.95	17.15	0.29	0.19	
I–In	42.87	48.87	8.26	–	–	0.53	Alloyed Mg_2NiH_4
I–In–0.26C	38.54	43.93	7.42	10.11	0.26	0.53	

Eleven alloys were prepared of an average chemical composition listed in Table 1. The ball-milled powder blend was compacted at room temperature into cylindrical pellets, the diameter and height of which were 20 and 4 mm, respectively. The pellets were annealed in Ar (purity 99.9999%) at 630 K for 20 h. Annealing was carried out under Ar pressure of 2 mbar to suppress oxidation and to prevent Mg evaporation.

The structure of the samples was observed by SEM JEOL JSM 6460 equipped with the EDAX/WEDAX Oxford Instruments analyzer. XRD patterns were obtained by the X'Pert Pro MPD device using CoKα radiation and the results were interpreted (Rietveld analysis) with the HighScore Plus SW and ICSD databases [58].

2.2. Hydrogen charging and desorption

The samples for desorption measurements were hydrided by annealing in gaseous hydrogen (purity 99.9999%, pressure 30 bars) at temperature T_c = 620 K for 20 h. This optimum charging temperature was found in a series of hydrogen charging experiments. It was verified that longer charging times at T_c = 620 K did not lead to a higher content of hydrogen. The hydrogen storage capacity was measured by precise weighing of samples, whose typical total mass was about 2 g.

The desorption of hydrogen was measured in isothermal regime in a Sieverts-type apparatus that was described in detail elsewhere [39]. The pressure $p(t)$ of desorbed hydrogen at desorption time t was measured by a piezoelectric gauge with a sampling frequency of 10 s. Knowing the volume of the desorption chamber (about 5 l) and the desorption temperature, the mass of desorbed hydrogen was calculated. The mass of each individual sample for low-temperature desorption experiments was chosen so that the final total hydrogen pressure in the chamber was well below the hydrogen equilibrium pressure of respective hydrides [59].

The desorption experiments were carried out at temperatures ranging from 458 to 640 K. The desorption temperature T was measured by a Pt/Pt-10Rh thermocouple that was in contact with the sample and stabilized within ±1 K. The samples were moved into the hot zone of the tempered furnace at the beginning and returned into the cold zone after the anneal so the initial and final temperature changes of the sample were always very short compared to the desorption time period needed for the total isothermal hydrogen desorption.

The desorption curves were measured immediately after hydrogen charging (minimum ageing time designated as τ_0) and the measurement was repeated with other samples of the same hydrogen-charged alloy after specified ageing times τ.

3. Results and discussion

3.1. Optimum conditions for hydrogen charging

Experimental samples were hydrogen-charged from a H_2-gas phase. The isothermal charging was carried out under a constant hydrogen pressure p_c that was always higher than the equilibrium hydrogen pressure p_{eq}, which is represented by the hydride dissociation pressure in a PCT diagram at respective charging temperature T_c (see, e.g., in [59]). Bearing in mind the decreasing course of the $\alpha + \beta/\beta$ interphase boundary in the PCT diagram [60], it is clear that higher values of c should be reached at lower temperatures T_c. However, due to the charging kinetics, the charging time t_c, which is needed to reach the maximum value of c_{max} at low charging temperatures can be too long for practical application and, hence, a reasonable charging regime has to be found.

Hydrogen concentration in the sample, c, measured for various values of t_c, increased initially with p_c and T_c (Figs. 1 and 2). In Fig. 1, the hydrogen concentration c is plotted in dependence on T_c for chosen experimental alloys. As a reasonable charging time, t_c, 20 h was chosen. It is obvious from Fig. 1 that with T_c increasing, the maximum value of c_{max} can be reached which corresponds to the equilibrium chemical composition on the $\alpha + \beta/\beta$ interphase boundary in the PCT diagram. A further increase in T_c (and constant values of p and t_c) leads to a decrease in c_{max} and, above a certain maximum temperature (critical temperature T_{crit} in PCT diagram), the β phase can no longer exist and, hence, no hydrogen can be stored in the alloy [60]. In the present work, optimum hydrogen charging conditions were used for all experimental alloys: $T_{c,optim}$ = 620 K, p_c = 30 bar and t_c = 20 h.

It is clear from Fig. 1 that an admixture of In and carbon led to a beneficial effect on the hydrogen charging kinetics: c_{max} is reached much more easily when the alloy's chemical composition is modified by In and C. An improvement of hydrogen desorption kinetics by In in binary Mg–In alloys was reported, e.g., in [61,62].

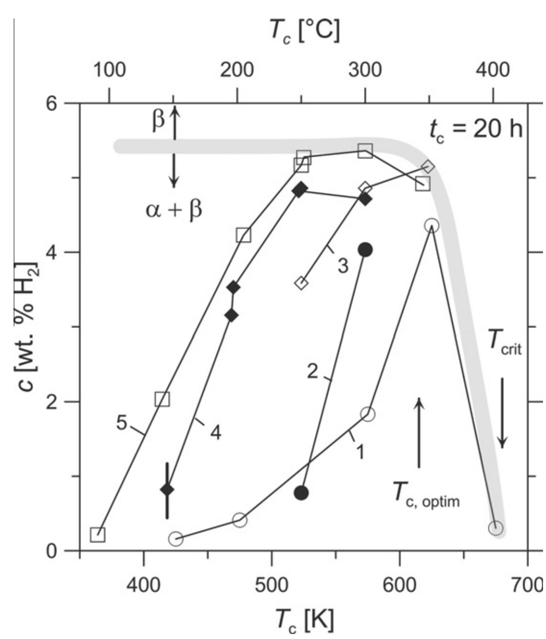

Fig. 1. Hydrogen concentration achieved after hydrogen charging at temperature T_c for time t_c = 20 h. 1 – E, 12.5 bar H_2; 2 – E–In, 2 bar H_2; 3 – E-In, 30 bar H_2; 4 – E–In–0.14C, 2 bar H_2; 5 – E–In–0.14C, 30 bar H_2. The limiting cover curve represents maximum hydrogen concentration at the $(\alpha + \beta)/\beta$ phase boundary in the PCT diagram [60]. Error bar – typical experimental error.

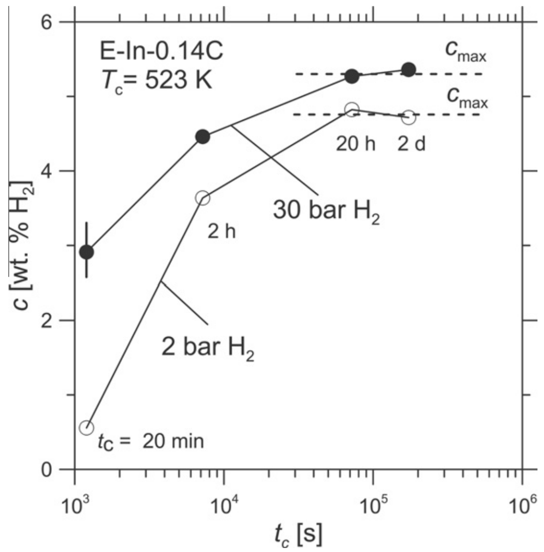

Fig. 2. Hydrogen concentration in E–In–0.14C achieved after hydrogen charging at temperature T_c = 523 K after charging for time t_c. Error bar – typical experimental error.

3.2. Estimation of maximum hydrogen desorption pressure

The equilibrium hydrogen pressure p_{eq} is an important parameter of a hydrogen storage material, since it is the limiting value of maximum pressure p_{max} ($p_{max} \leqslant p_{eq}$) of desorbed hydrogen at chosen temperature T_c. To obtain an assessment of p_{eq}, the hydrogen pressure on the $\alpha/(\alpha + \beta)$ interphase boundary [60] was measured in the rising-temperature regime for alloys E, E–In and E–In–xC. The obtained values are close to the dissociation pressure of MgH_2 (it is the lower PCT plateau of the $MgH_2 + Mg_2NiH_4$ mixture of hydrides [63]). The results are plotted in Fig. 3 together with literature values of dissociation pressure p_{eq} published for MgH_2 and Mg_2NiH_4 hydrides [59]. A typical standard deviation σ (probability level 68.2%) of the calculated values of p_{max} was about 5%, which was within the size of the points in Fig. 3. Due to the experimental scatter of the observed p_{max} measured with E–In–xC alloys (at two lowest temperatures, the values of p_{max} fell outside the interval ±σ), no significant dependence of p_{max} on carbon concentration x was observed. It can be seen in Fig. 3 that the presence of In and C causes p_{max} to reach higher values, which is beneficial from the point of view of possible technology applications.

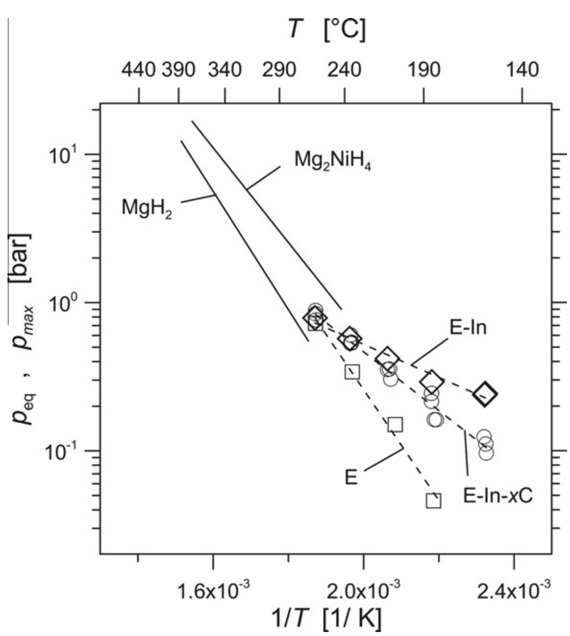

Fig. 3. Measured maximum hydrogen pressure p_{max} (points and dashed straight lines) plotted together with literature values of equilibrium dissociation pressure p_{eq} [59] (solid straight lines).

3.3. XRD phase analysis

Two XRD patterns for minimum and maximum concentrations of carbon c_C in E–In–xC alloys shown in Fig. 4 illustrate two main features of the obtained results: They document that (i) MgH_2 is the majority hydride phase in E–In–xC alloys and (ii) that there is a crowding-out effect. The latter was observed for higher values of c_C, where In and Ni components precipitated either as pure elements, or as Mg_3In compound. This is shown quantitatively in Fig. 5, where it can be seen that the amount of Mg_2NiH_4 (β) + Mg_2NiH_3 (α) decreased slightly whereas the amount of MgH_2 increased with the increasing of carbon-to-magnesium concentration ratio $x = c_C/c_{Mg}$. It can also be seen that Ni and In are partly crowded-out by carbon from the hydrogen-charged, mechanically alloyed, ball-milled Mg–Ni–In mixture. A precipitation of three new phases of alloys with x > 0.7 caused a decrease in hydrogen storage capacity c_{max} (Fig. 5). Interestingly, the ratio of non-microtwinned and microtwinned low-temperature phases of Mg_2NiH_4 ([64]), LT1/LT2, increased with x increasing.

Calculation of a size-broadening factor allowed for an estimate of the mean crystallite size d_c. It can be seen in Fig. 6 that d_c values were lower in Mg_2NiH_4 than the values measured in MgH_2. In both cases, d_c decreased with increasing carbon concentration $x = c_C/c_{Mg}$. The dependence is relatively strong for the MgH_2 phase within the concentration interval of x < 0.7. The decreasing dependence of d_c on increasing x is most likely caused by the dislocation pinning by carbon, which implies formation of finer crystallites. The presence of In did not seem to affect the value of d_c significantly. A typical standard deviation of values of d_c obtained from the Rietveld analysis was about 5% (σ). The observed scatter of repeatedly measured points is in some cases outside the interval ±σ due to the influence of other factors (measurement with different alloys, etc.).

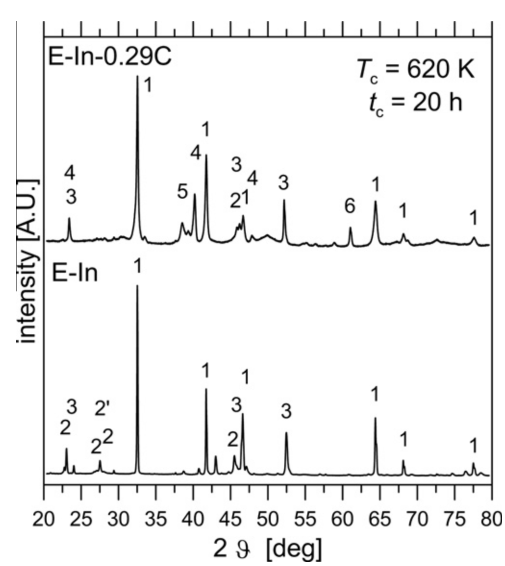

Fig. 4. XRD pattern measured with hydrogenated E–In–xC alloys containing minimum (x = 0) and maximum (x = 0.29) carbon concentration. 1 – MgH_2, 2 – Mg_2NiH_4 LT1, 2' – Mg_2NiH_4 LT2, 3 – $Mg_2NiH_{0.3}$, 4 – Mg_3In, 5 – In, 6 – Ni.

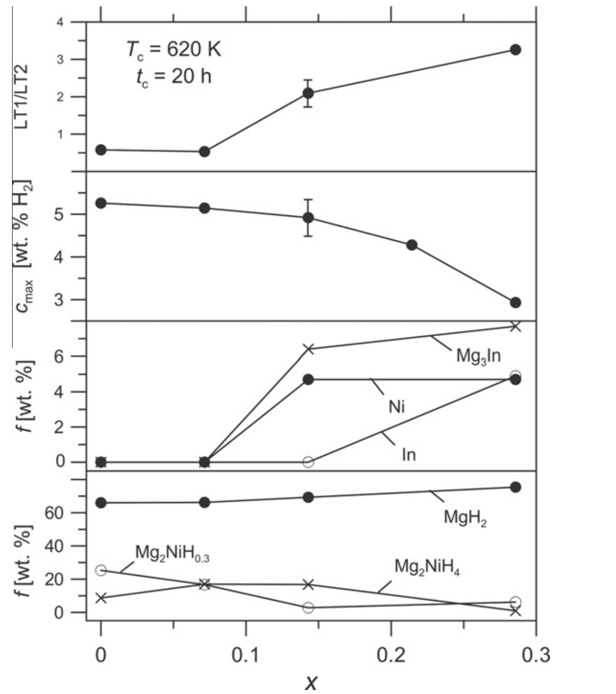

Fig. 5. Phase composition f, hydrogen storage capacity c_{max} and ratio of un-twinned (LT1) and twinned (LT2) modification of Mg_2NiH_4 low-temperature phase in E–In–xC alloys. Error bars – typical experimental error.

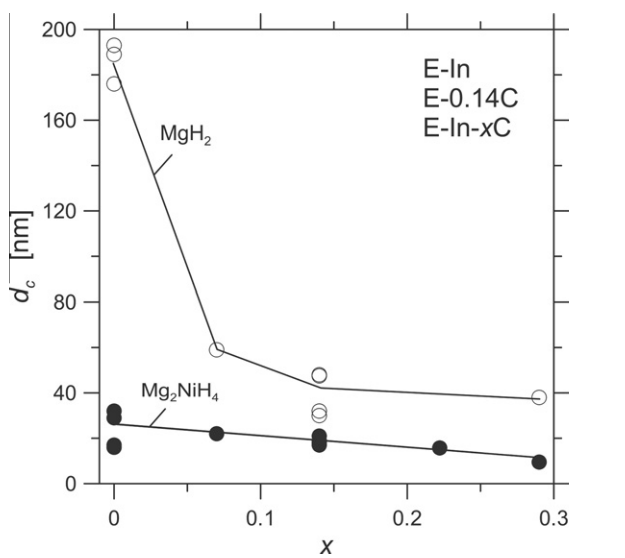

Fig. 6. Mean size of XRD domains in principal phase components MgH_2 and Mg_2NiH_4 of E–In–xC alloys.

3.4. Desorption experiments

Examples of desorption curves measured with eutectic and alloyed eutectic are shown in Fig. 7. The measurements were carried out at a constant desorption temperature T from the temperature range of 430–640 K; the desorption time t_c varied from 10^2 s to about 3×10^5 s. The desorption experiments performed at the lowest temperatures were interrupted before achieving a totally desorbed state due to the extremely long values of t_c needed to complete desorption.

3.4.1. Influence of chemical composition

To compare the desorption rates for various experimental alloys, time $t_{0.5}$ was introduced *ad hoc*. Within this time, one half of hydrogen stored was desorbed. The plot of $t_{0.5}$ vs. desorption temperature T obtained for freshly hydrogen-charged (time τ_0) alloys is shown in Fig. 8. It was proven that time $t_{0.5}$ remained unchanged within ±5% in repeated desorption experiments carried out at the same desorption temperature and after the same ageing time τ. Hence, the experimental error of $t_{0.5}$ values plotted in Fig. 8 in co-ordinates log $t_{0.5}$ vs. T is comparable with the size of points. The plot in Fig. 8 classifies the desorption behavior of the studied alloys: It can be observed that the hydrogen desorption rate of a non-alloyed eutectic E (crosses) was the lowest. It should be noted that the value of $t_{0.5}$ obtained for E and for the lowest desorption temperature is underestimated because of ageing (see the next paragraph) during long desorption experiment itself. The actual value of $t_{0.5}$ could be expected a little higher, as indicated by the dotted line in Fig. 8.

It can be clearly seen that the values of $t_{0.5}$ obtained for alloy E at two lowest temperatures are significantly higher than those that could be expected from a high-temperature extrapolation. This additional low-temperature inhibition can be suppressed by In. It is obvious from Fig. 8 that the introduction of In improves the desorption kinetics significantly at temperatures approximately below 590 K. This improvement most likely originates in the catalyst effect or in the oxidation suppression [40]. The beneficial effect of In observed in the present work is in agreement with the results reported in [61,62] for similar materials. It is worth noting that the beneficial effect of In occurs to effect just in the temperature range which may be important for potential technology application. One can see in Fig. 8 that alloying by In did not impart any significant improvements in hydrogen desorption kinetics to alloy E at higher desorption temperatures where the desorption process runs sufficiently fast without any stimulation of In added.

Addition of carbon led to another beneficial contribution to hydrogen desorption acceleration. It is clear from Fig. 8 that all studied freshly hydrogen-charged carbon-containing E–In–xC alloys desorbed hydrogen faster than alloys without carbon. However, the accelerating effect of carbon is not proportional to the amount x of carbon added to the E–In alloy. The optimum acceleration of hydrogen desorption (the lowest values of $t_{0.5}$) was observed for x = 0.7. A further increase in carbon content led to a slight deceleration of hydrogen desorption.

This observation, which is in qualitative agreement with the conclusions drawn in [57] for hydrogen absorption in a similar alloy $(Mg–V)_{nano}$, can be rationalized with the help of our results on XRD study – see in Fig. 5. It was observed that a higher content of carbon (x > 0.7) caused a phase decomposition of hydrogen storage alloys, since new phases (pure In, Ni and a Mg_3In compound) appeared after hydrogen charging. The phase decomposition at x > 0.7 shows detrimental effect on the hydrogen storage characteristics ($t_{0.5}$ and c_{max}), since In and Ni, which ensure a desired catalytic effect, are drawn to build new phases that are neutral with respect to the hydrogen storage efficiency.

Interestingly, carbon stabilized the catalyzing Mg_2NiH_4 phase, which is illustrated in Fig. 9 for I–In–0.26C and I–In alloys. The fact that hydrogen desorption from Mg_2NiH_4 catalyzing phase does not depend on τ ensures its catalyzing effect [40] for a longer time than expected in alloys without carbon.

The hydrogen desorption rate was also influenced by the Mg:Ni ratio. It is illustrated in Fig. 10 that an increasing amount of Ni resulted in acceleration of the hydrogen desorption rate. This effect originates in the content of the Mg_2NiH_4 catalyzing phase which increased with the increasing Ni concentration. The improvement of the desorption kinetics was, however, outweighed by a lower specific hydrogen storage capacity due to a higher specific weight of the alloy.

We found that presence of In did not significantly improve the hydrogen desorption kinetics in samples alloyed by carbon, as

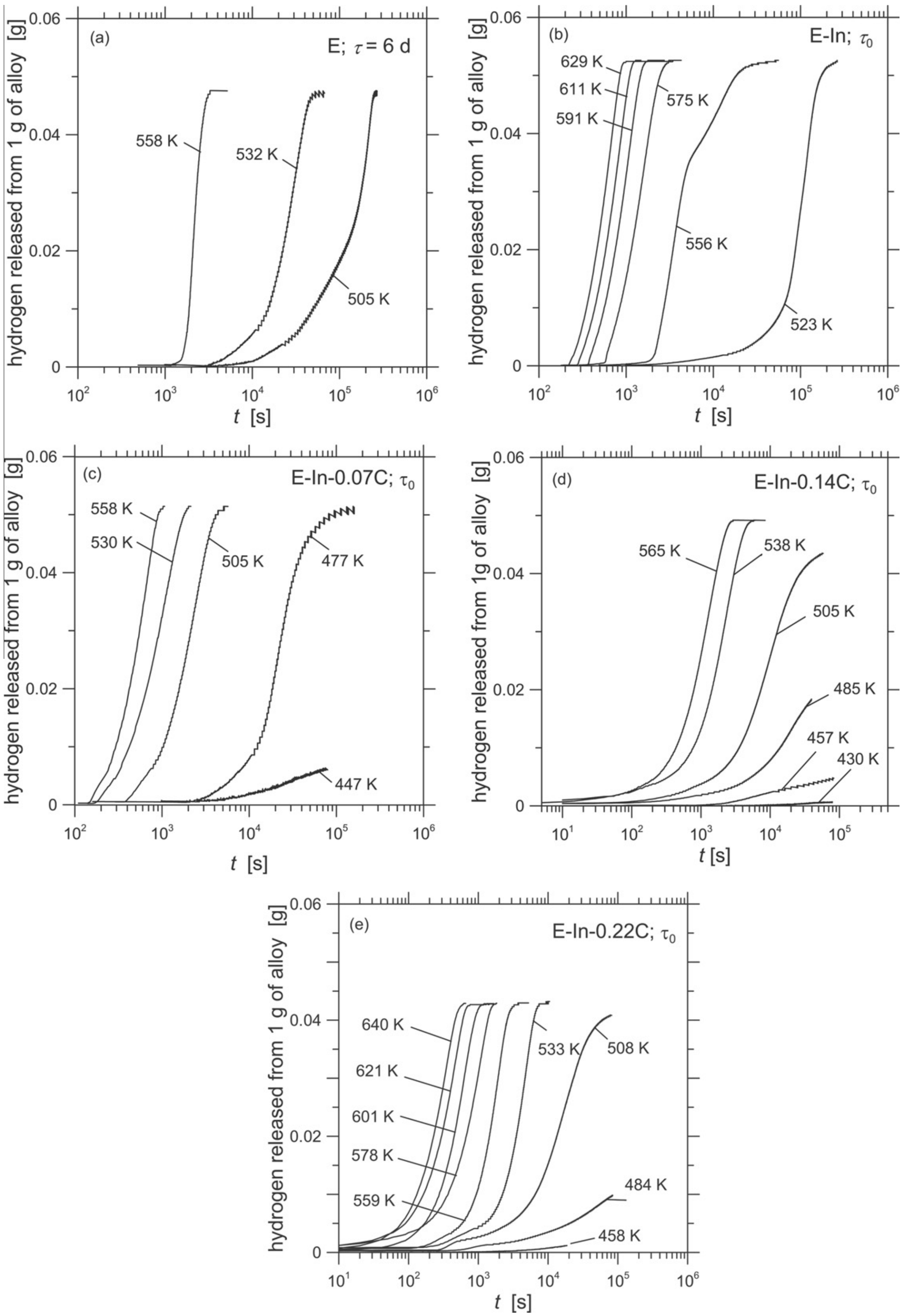

Fig. 7. Examples of desorption curves measured with alloys E (a), E–In (b), E–In–0.07C (c), E–In–0.14C (d) and E–In–0.22C (e).

compared to the desorption kinetics in samples containing carbon only. This is documented in Fig. 11, where it can be seen that the values of $t_{0.5}$ for both alloys with carbon are very close to each other. However, the beneficial effect of In in alloys with carbon was primarily in the fact that it effectively prevented oxidation of samples with carbon.

3.4.2. Ageing

In a series of subsequent desorption experiments performed with samples of the same alloy, time $t_{0.5}$ decreased in dependence on the duration of room-temperature ageing, τ. It is illustrated in Fig. 12 for alloys E, E-In and E-In–0.07C (for the mechanism of ageing, see in [65]). One can see that the E–In alloy showed the

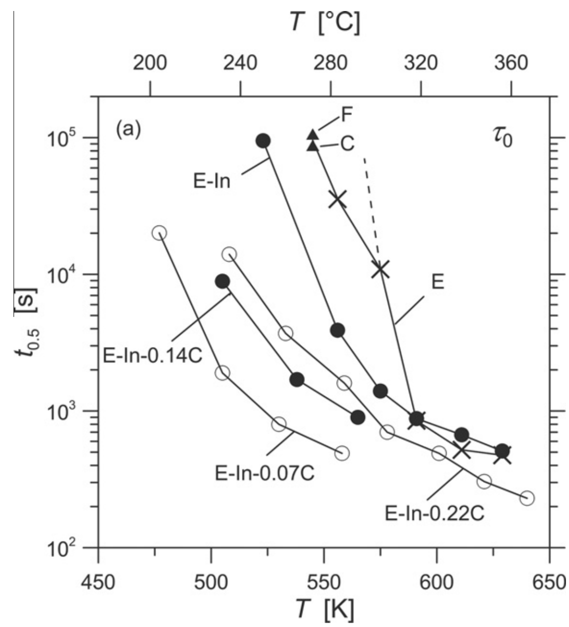

Fig. 8. Comparison of hydrogen desorption kinetics measured immediately after hydrogen charging. F, C – finer and coarser fraction of ball-milled alloy E, respectively.

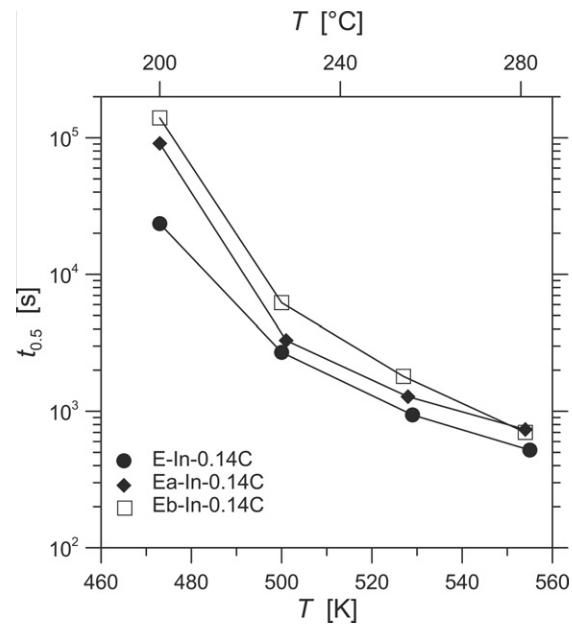

Fig. 10. Comparison of hydrogen desorption kinetics measured with E–In–0.14C alloys: influence of Mg/Ni ratio.

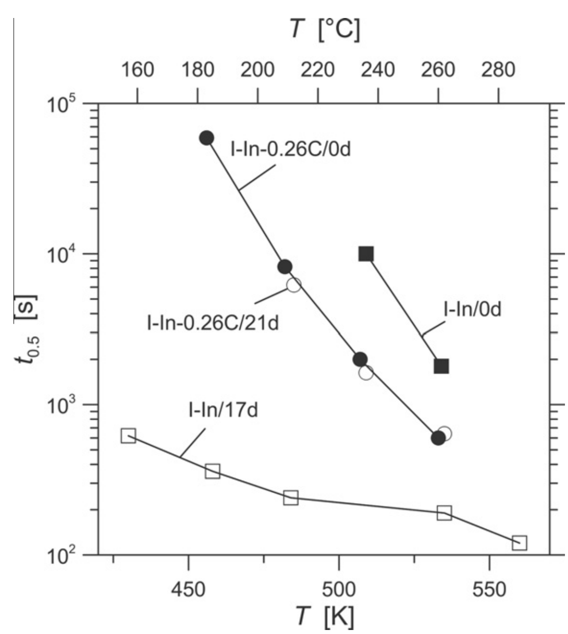

Fig. 9. Comparison of hydrogen desorption kinetics measured with I–In–xC alloys: influence of carbon and τ.

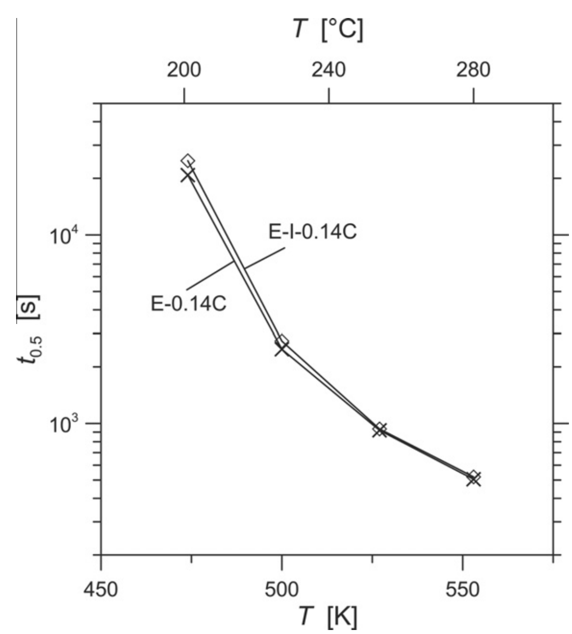

Fig. 11. Comparison of hydrogen desorption kinetics: influence of In in carbon-containing alloy.

same desorption behavior immediately after hydrogen charging (at time τ_0 = 0 days) as the E alloy did after a time of about τ = 9 days (cf. curves E–In/0d and E/9d). The addition of In considerably shortened $t_{0.5}$ at temperatures below approximately 580 K, which is obvious while comparing the E–In/0d and the E/0d curves. After a rapid change (decrease in $t_{0.5}$) of the desorption curves observed with alloys E, E–In within the first 9 days, its ageing went on very slowly and reached an almost fully aged state (no further change of $t_{0.5}$ after an extremely long ageing time) after the time of about $\tau \cong 90$ days when the values of $t_{0.5}$ became close to the values of $t_{0.5}$ measured for E–In–0.07C alloy at τ_0 (cf. point E–In/92d with values measured for E–In–0.07C/0d).

Alloys modified by carbon showed the ageing effect, too. However, their fully aged state was reached much earlier as is illustrated in Fig. 12. Above the temperature of approximately 480 K, the E–In–0.07C alloy reached its stationary state immediately after hydrogen charging (cf. curves for alloy E–In–0.07C desorbed at times τ_0 and τ = 54 days).

It is likely that the desorption curves for any E-type alloy (i.e., Mg–Ni eutectic modified by In and C) reach a certain limiting position in co-ordinates $t_{0.5}$ vs. T after a sufficient ageing period τ (i.e. they converge in the shaded area in Fig. 12). This limiting state seems to be an optimum for an E-type hydrogen storage material, characterized by very rapid hydrogen desorption. It was found that

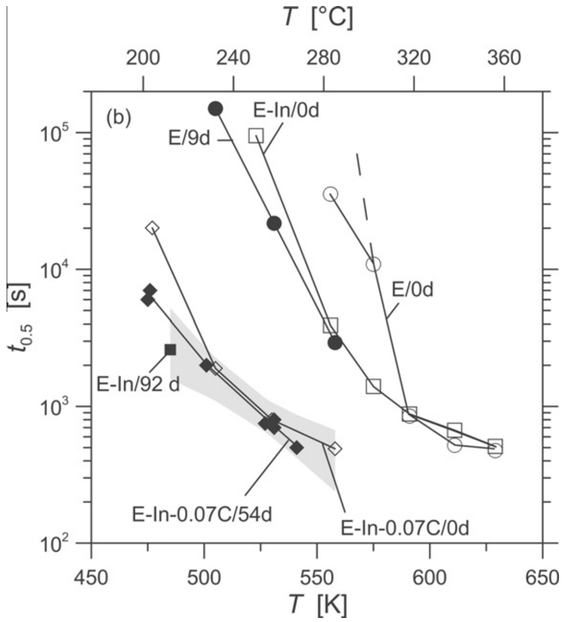

Fig. 12. Comparison of hydrogen desorption kinetics: influence of τ. Shaded area – see text.

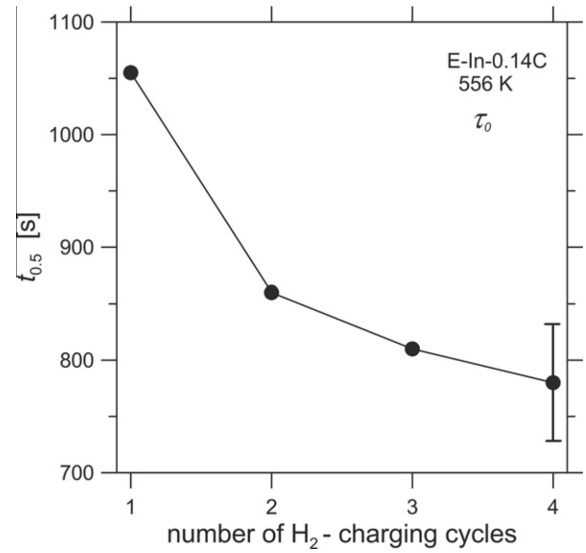

Fig. 13. Comparison of hydrogen desorption kinetics in the first four hydrogen charging/discharging cycles.

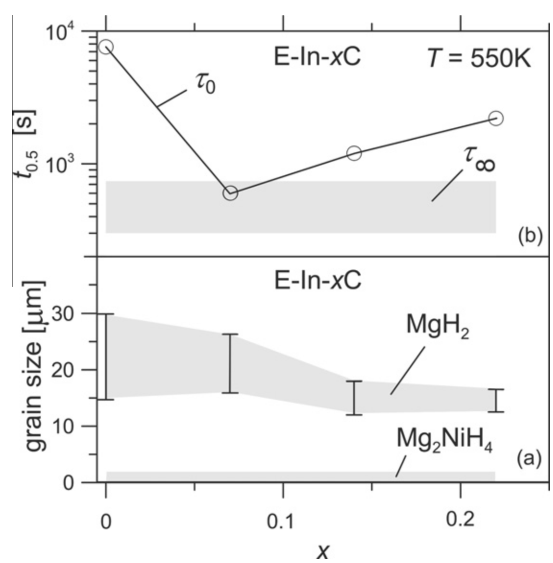

Fig. 14. Grain size (a) and hydrogen desorption time $t_{0.5}$ for desorption temperature $T = 550$ K (b) in dependence on carbon content in E–In–xC alloy. τ_0, τ_∞ – measured immediately after hydrogen charging and after a very long ageing time, respectively.

this state is immediately reachable (without ageing) when the concentration of carbon is close to its optimum value of 5 wt.% (alloy E–In–0.07C).

Assuming the hydrogen desorption described by the dependence of $t_{0.5}$ on T is controlled by a thermal-activated process of the Boltzmann-type, the dependence of $t_{0.5} \sim \exp(Q/RT)$ can be fitted to the experimental points. Fitting the points obtained for E-In/92d, E–In–0.07/54d and E–In–0.07C/0d (i.e. points close to fully aged state) led to the activation enthalpy $Q = (60 \pm 6)$ kJ/mol H_2. The shaded area in Fig. 12 represents a confidence interval of 99.9% for the fit.

3.4.3. Cycling

It was observed that another decrease in $t_{0.5}$ can be achieved after several hydrogen charging/discharging cycles. This activation of the hydrogen storage capability of the material is illustrated in Fig. 13 for the E–In–0.14C alloy. It was found that four cycles are sufficient for an effective activation of this HSM. A further decrease of the $t_{0.5}$ value was less than the scatter of experimental results only after the first four cycles. The observed effect may be – at least partially – caused by the cracking of great MgH_2 grains, which effectively resulted in a decrease in the mean grain size.

3.4.4. Effect of carbon on hydrogen desorption

It was frequently concluded in the literature (see, e.g., in [54]) that the beneficial effect of carbon on ball-milled hydrogen storage materials is caused *mainly* by its *anti-sticking* effect. In other words, it is believed that carbon prevents conglomeration of particles of the milled blend which results in their lower mean grain size. Measurement of grain size in hydrogen charged E–In–xC alloys confirmed a weak decrease in the grain size of MgH_2 only with increasing carbon content: Shaded areas in Fig. 14a capture the obtained values of grain size of about 90% of grains. It is clear that the grain size of MgH_2 is greater than that of Mg_2NiH_4 and that it decreases slightly with increasing x, while the grain size of Mg_2NiH_4 seems to be unaffected by the presence of carbon.

In Fig. 14b, the dependence of $t_{0.5}$ on x is plotted for temperature $T = 550$ K. The line represents the values of $t_{0.5}$ measured immediately after hydrogen charging (τ_0), the shaded area represents the expected limit values of $t_{0.5}$ for a fully aged state (τ_∞). The area corresponds to the range of the confidence interval in Fig. 12 at temperature $T = 550$ K. Comparing Fig. 14a and b, it is obvious that there is no simple relation between the grain size and hydrogen desorption kinetics scaled by $t_{0.5}$ – both taken with the same carbon content x.

It may be concluded that the hydrogen desorption rate at τ_0 is not *primarily* controlled by the geometrical size of particles in the ball-milled powder. It can be easily deduced that the same conclusion can be drawn also when the mean size of domains d_c (see in Fig. 6) is considered instead of the mean grain size (Fig. 14a) as the characteristic size of particles.

To prove the above conclusion that the grain size is not the main and/or unique factor influencing the hydrogen desorption kinetics immediately after hydrogen charging, two desorption experiments were done with two size fractions of milled alloy E at temperature T = 545 K. The fine fraction (F) consisted of grain sizes from 40 to 100 μm (34.3 wt.% of the milled blend), the coarse fraction (C) consisted of particles of grain sizes from 100 to 250 μm (52.8 wt.%). Both fractions, separated by sieving, were compacted into pellets and hydrogen charged as described above. From the desorption tests done for ageing time τ_0, times $t_{0.5,F} = 1.03 \times 10^5$ s and $t_{0.5,C} = 8.5 \times 10^4$ s were obtained for the F and C fractions, respectively. Values of $t_{0.5,F}$ and $t_{0.5,C}$ agree reasonably well with an extrapolation of values obtained for non-separated samples E at higher desorption temperatures (see crosses in Fig. 8). However, the obtained relation $t_{0.5,F} > t_{0.5,C}$ reflects a slightly different stage of ageing of the F and C fractions rather than a consequence of difference in effective grain size, since a reversed relation $t_{0.5,F} < t_{0.5,C}$ should be expected: If the simple *out-gassing* model is accepted in the first approximation, an analytical solutions of a related case, i.e. out-gassing from a cube or from a sphere into a closed volume [66,67], predict a relation of $t_{0.5} \sim 1/\rho^2$ (ρ stands for the characteristic linear size of the degassing body).

Based on the above reasoning, it may by concluded that the observed improvement of the hydrogen desorption kinetics from carbon-containing alloys is not a consequence of carbon-induced refinement of the mean grain size of ball-milled samples. It is most likely that other effects declared in the literature come into play, such as enhanced resistance to surface oxidation caused by the presence of carbon [53,55,57] and, above all, the catalytic effect of carbon [51,52,56].

The limitation of the beneficial effect of carbon ($c_C \leqslant 5$ wt.%) is most likely due to the precipitation of unwanted phases with higher carbon contents (see in Fig. 5). The presence of these phases leads to the downgrading of the hydrogen desorption kinetics and hydrogen storage capacity for higher carbon contents ($c_C > 5$ wt.%).

4. Conclusions

In the present paper, the influence of carbon additions to ball-milled Mg–Ni-based alloys, containing In to prevent oxidation, on the hydrogen desorption kinetics was investigated. It was observed that carbon improves the hydrogen desorption kinetics significantly. The optimum of its beneficial effect was found close to the carbon concentration of about $c_C \cong 5$ wt.% C. For the optimum composition, the onset of hydrogen desorption at temperatures above 485 K occurs immediately after hydrogen charging. This shortens substantially the hydrogen charging/discharging cycle of storage tanks that use Mg–Ni-based alloys as the hydrogen storage medium.

The study of grain size influence (controlled either by the carbon content or by fractioning the milled powders by sieving) on hydrogen desorption led to a conclusion that there is no significant improvement of the hydrogen desorption rate caused by gain refinement. Nevertheless, the beneficial effect of carbon on hydrogen desorption kinetics was observed for alloys with carbon content up to $c_C \cong 5$ wt.% C. It can be ascribed to the catalyzing phase stabilization of by carbon, as it was reported in Ref. [40], or to the contribution of carbon to an easier formation of bridges of rapid hydrogen desorption [65]. Better hydrogen desorption kinetics from alloys with carbon may also originate in the catalytic effect of carbon itself [51,53] and/or in the enhancement of the surface oxidation resistance by carbon [55,56]. It was also observed that carbon increases the maximum pressure of desorbed hydrogen at given temperature.

For carbon concentrations above $c_C \cong 5$ wt.% C, unwanted phases precipitated, which most likely led to downgrading of hydrogen desorption kinetics and hydrogen storage capacity, since the elements which improve the desired hydrogen storage features (Ni and In) were withdrawn from the phases useful for hydrogen storage, forming new phases that are ineffective for hydrogen storage.

Acknowledgments

This work was supported by projects GACR 106/09/0814, GACR P108/11/0148, AV 0Z20410507 and CEITEC CZ.1.05/1.1.00/02.0068. The authors are very grateful to Mr. B. David for assistance with the XRD measurement.

References

[1] G. Sandrock, J. Alloys Compd. 293–295 (1999) 877–888.
[2] G. Walker (Ed.), Solid-State Hydrogen Storage, Woodhead Publishing Ltd., Cambridge, 2008.
[3] L. Schlapbach (Ed.), Topics in Applied Physics – Hydrogen in Intermetallic Compounds II, Springer-Verlag, Berlin, Heidelberg, New York, London, Paris, Tokyo, Hong Kong, Barcelona, Budapest, 1992.
[4] M. Fichtner, J. Alloys Compd. 509S (2011) S529–S534.
[5] M. Hirscher (Ed.), Handbook of Hydrogen Storage, Wiley-VCH Verlag, Weinheim, 2010.
[6] B. Sakintuna, F. Lamari-Darkrim, M. Hirscher, Int. J. Hydrogen Energy 32 (2007) 1121–1140.
[7] I.P. Jain, C. Lal, A. Jain, Int. J. Hydrogen Energy 35 (2010) 5133–5144.
[8] T. Czujko, Z. Zaranski, I.E. Malka, Z. Wronski, J. Alloys Compd. 509 (2011) S604–S607.
[9] H.C. Zhong, H. Wang, L.Z. Ouyang, M. Zhu, J. Alloys Compd. 509 (2011) 4268–4272.
[10] P. Larsson, C. Moyses-Araujo, J.A. Larson, P. Jena, R. Ahuja, Proc. Natl. Acad. Sci. USA 105 (2008) 8227–8231, http://dx.doi.org/10.1073/pnas.0711743105.
[11] S. Li, P. Jena, R. Ahuja, Phys. Rev. B 74 (2006), http://dx.doi.org/10.1103/PhysRevB.74.132106-4. Article ID 132106, 4 page.
[12] A. Zaluska, L. Zaluski, J.O. Stroem-Olsen, Appl. Phys. A 72 (2001) 157–165.
[13] Y. Jia, L.N. Cheng, N. Pan, J. Zou, G.Q. Lu, X.D. Yao, Adv. Energy Mater. 1 (2011) 387–393.
[14] S. Aminorroaya, A. Ranjbar, Y. Cho, H. Liu, A. Dahle, Ceram. Trans. 224 (2011) 17–24.
[15] A.R. Yavari, G. Vaughan, F. Ribeiro de Castro, K. Georgarakis, A.M. Jorge Jr., I. Nuta, W.J. Botta, J. Alloys Compd. 540 (2012) 57–61.
[16] J. Bellemare, J. Huot, J. Alloys Compd. 512 (2012) 33–38.
[17] J. Mao, Z. Guo, X. Yu, H. Liu, J. Alloys Compd. 509 (2011) 5012–5016.
[18] X. Ye, Y. An, G. Xu, J. Alloys Compd. 509 (2011) 152–156.
[19] I.E. Malka, J. Bystrycki, T. Plocinski, T. Czujko, J. Alloys Compd. 509S (2011) S616–S620.
[20] H. Hirate, M. Morinaga, H. Yukawa, H. Nakai, J. Alloys Compd. 509S (2011) S612–S615.
[21] A. Montone, A. Aurora, D.M. Gatia, M.V. Antisari, Scr. Mater. 63 (2010) 456–459.
[22] M.V. Antisari, A. Aurora, D.M. Gatia, A. Montone, Scr. Mater. 61 (2009) 1064–1067.
[23] C. Milanese, A. Girella, G. Bruni, P. Cofrancesco, V. Berbenni, P. Matteazzi, A. Marini, Intermetallics 18 (2010) 203–211.
[24] R.W. Denis, I.Yu. Zavaliy, V. Paul-Boncour, V.V. Berezovets, I.V. Kovalchuk, A.B. Riabov, Intermetallics 18 (2010) 1579–1585.
[25] N. Bazzanella, R. Checchetto, A. Miotello, J. Nanomater. (2011), http://dx.doi.org/10.1155/2011/865969. Article ID 865969, 11 page.
[26] Y. Zhu, Y. Yang, L. Wei, Z. Zhao, L. Li, J. Alloys Compd. 520 (2012) 207–212.
[27] S.A. Pighin, C. Capurso, S. lo Russo, H.A. Peretti, J. Alloys Compd. 530 (2012) 111–115.
[28] X.B. Yu, Z.X. Yang, H.K. Liu, D.M. Grant, G.S. Walke, Int. J. Hydrogen Energy 35 (2010) 6338–6344.
[29] R.R. Shahi, T.P. Yadav, M.A. Shaz, O.N. Srivastva, Int. J. Hydrogen Energy 35 (2010) 238–246.
[30] H. Simchi, A. Kaflou, A. Simchi, Int. J. Hydrogen Energy 34 (2009) 7724–7730.
[31] M. Polanski, J. Bystricki, T. Plocinski, Int. J. Hydrogen Energy 33 (2008) 1859–1867.
[32] F. Tonus, V. Fuster, G. Urretavizcaya, F.J. Castro, J.-L. Bobet, Int. J. Hydrogen Energy 34 (2009) 3404–3409.
[33] Y.-H. Zhang, B.-W. Li, H.-P. Ren, F. Hu, G.-F. Zhang, S.-H. Guo, J. Alloys Compd. 509 (2011) 5604–5610.
[34] Y. Zhu, C. Yang, J. Zhu, L. Li, J. Alloys Compd. 509 (2011) 3514–5309.
[35] Y.-H. Zhang, F. Hu, S.-G. Li, K. Lu, S.-H. Guo, X.-L. Wang, J. Alloys Compd. 509 (2011) 294–300.
[36] Y-H. Zhang, B-W. Li, H-P. Ren, X-X. Ding, X-G. Liu, L-L. Chen, J. Alloys Compd. 509 (2011) 2808–2814.
[37] Y. Wu, M.W. Lototsky, J.K. Solberg, V.A. Yartys, J. Alloys Compd. 509 (2011) S640–S645.
[38] X. Yang, N. Takeichi, K. Shida, H. Tanaka, N. Kuriyama, T. Sakai, J. Alloys Compd. 509 (2011) 1211–1216.
[39] J. Cermak, L. Kral, Acta Mater. 56 (2008) 2677–2686.
[40] J. Cermak, B. David, Int. J. Hydrogen Energy 36 (2011) 13614–13620.
[41] J. Cermak, L. Kral, J. Power Sources 197 (2012) 116–120.
[42] F.J. Castro, V. Fuster, G. Urretavizcaya, J. Alloys Compd. 509S (2011) S595–S598.
[43] Y. Jia, Y.N. Guo, J. Zou, X.D. Yao, Int. J. Hydrogen Energy 37 (2012) 7579–7585.
[44] A.D. Rud, A.M. Lakhnik, Int. J. Hydrogen Energy 37 (2012) 4179–4187.

[45] H. Gasan, O.N. Celik, N. Aydinbeyli, Y.M. Yaman, Int. J. Hydrogen Energy 37 (2012) 1912–1918.
[46] V. Fuster, F.J. Castro, H. Troiani, G. Urretavizcaya, Int. J. Hydrogen Energy 36 (2011) 9051–9061.
[47] G. Urretavizcaya, V. Fuster, F.J. Castro, Int. J. Hydrogen Energy 36 (2011) 5411–5417.
[48] P. Adelhelm, P.E. de Jongh, Int. J. Hydrogen Energy 21 (2011) 2417–2427.
[49] S.X. Zhou, H.L. Niu, H.P. Chen, S.S. Lu, C. Zhang, L.Y. Feng, Q.D. Zhang, Adv. Mater. Res. 239–242 (2011) 69–72.
[50] D.N. Borisov, P.V. Fursikov, B.P. Tarasov, Int. J. Hydrogen Energy 36 (2011) 1326–1329.
[51] H. Imamura, M. Kusuhara, S. Minami, M. Matsumoto, K. Masanari, Y. Sakata, K. Itoh, T. Fukunaga, Acta Mater. 51 (2003) 6407–6414.
[52] H. Imamura, S. Tabata, N. Shigetomi, Y. Takesue, Y. Sakata, J. Alloys Compd. 330–332 (2002) 579–583.
[53] A. Montone, J. Grbovic, A. Bassetti, L. Mirenghi, P. Rotolo, E. Bonetti, L. Pasquini, M.V. Antisari, Mater. Sci. Forum 494 (2005) 137–142.
[54] Y. Zhu, Z. Liu, Y. Yang, H. Gu, L. Li, M. Cai, Int. J. Hydrogen Energy 35 (2010) 6350–6355.
[55] C.X. Shang, Z.X. Guo, J. Power Sources 129 (2004) 73–80.
[56] T. Spassov, Z. Zlatanova, M. Spassova, S. Todorova, Int. J. Hydrogen Energy 35 (2010) 10396–10403.
[57] S. Boucharia, P.P. Dodelet, D. Guay, J. Huot, R. Schulz, J. Mater. Res. 16 (2001) 2893–2905.
[58] Inorganic Crystal Structure Database (ICSD), Release 2011-2, Fachinformationszentrum Karlsruhe, Germany, and the National Institute of Standards and Technology (NIST), the US Department of Commerce, 2011 United States (CD-ROM).
[59] C. Weidenthaler, M. Felderhoff, Complex hydrides, in: M. Hirscher (Ed.), Handbook of Hydrogen Storage, Willey-VCH Verlag, Weinheim, 2010, pp. 117–151.
[60] J. Huot, Metal hydrides, in: M. Hirscher (Ed.), Handbook of Hydrogen Storage, Wiley-VCH Verlag, Weinheim, 2010, pp. 81–116.
[61] Z. Gavra, Z. Hadari, M.H. Mintz, J. Inorg. Nucl. Chem. 43 (1981) 1763–1768.
[62] H.C. Zhong, H. Wang, J.W. Liu, D.L. Sun, M. Zhu, Scr. Mater. 65 (2011) 285–287.
[63] R.B. Schwarz, MRS Bull. 24 (1999) 40–44.
[64] P. Zolliker, K. Yvon, Ch. Bearlocher, J. Less-Common Met. 115 (1986) 65–78.
[65] J. Cermak, L. Kral, J. Power Sources 214 (2012) 208–215.
[66] H.S. Carslaw, J.C. Jaeger, Conduction of Heat in Solids, Clarendon Press, Oxford, 1959. 176.
[67] J. Crank, The Mathematics of Diffusion, Clarendon Press, Oxford, 1957. 84.